

On the central stellar mass density and the inside-out growth of early-type galaxies

P. Saracco^{1*}, A. Gargiulo¹, M. Longhetti¹

¹INAF - Osservatorio Astronomico di Brera, Via Brera 28, 20121 Milano, Italy

Accepted 2012 February 25

ABSTRACT

Recent theoretical and observational studies on the assembly of early-type galaxies (ETGs) point towards an inside-out growth of their stellar mass characterized by extended low mass-density halos grown around compact and dense cores. Models can form ETGs at high- z as compact spheroids that then grow in size through dry minor mergers. Dry mergers would affect mainly the outskirts of the galaxy enlarging the size (i.e. the effective radius) keeping the inner parts and the total stellar mass nearly unchanged. Hence, the central stellar mass density will not change with time in contrast to the stellar mass density within the effective radius which should decrease with time as the effective radius increases. Some previous observations are interpreted as supporting inside-out growth as the central stellar mass density of high- z ETGs is found similar to that of local ETGs. In this paper we derive the central stellar mass density within a fixed radius and the effective stellar mass density within the effective radius for a complete sample of 34 ETGs morphologically selected at $0.9 < z_{spec} < 2$ and compare them with those derived for a sample of ~ 900 local ETGs in the same mass range. We find that the central stellar mass density of high- z ETGs spans just an order of magnitude and is similar to that of local ETGs, as found in previous studies. However, we find that the effective stellar mass density of high- z ETGs spans three orders of magnitude, exactly as the local ETGs and that it is similar to the effective stellar mass density of local ETGs showing that it has not changed since $z \sim 1.5$, in the last 9-10 Gyr. Thus, the wide spread of the effective stellar mass density observed up to $z \sim 1.5$ must originate earlier, at $z > 2$. Furthermore, we show that the small scatter of the central mass density of ETGs compared with the large scatter of the effective mass density is simply a peculiar feature of the Sersic profile and hence is independent of redshift and of any assembly history experienced by galaxies. Thus, it has no connection with the possible inside-out growth of ETGs. Finally, we show a tight correlation between the central stellar mass density and the total stellar mass of ETGs in the sense that the central mass density increases with mass as $\mathcal{M}_*^{-0.6}$. This implies that the fraction of the central stellar mass of ETGs decreases with the mass of the galaxy. These correlations are valid for the whole population of ETGs considered independently of their redshift suggesting that they originate in the early-phases of their formation.

Key words: galaxies: evolution; galaxies: elliptical and lenticular, cD; galaxies: formation; galaxies: high redshift

1 INTRODUCTION

The formation and the mass assembly history of early-type galaxies (ETGs; ellipticals and lenticulars) are central issues in the general topic of galaxy formation, issues that are not fully understood. Much effort has been devoted to understanding the formation and the evolution of ETGs in the context of hierarchical models of structure formation (e.g. Khochfar and Burkert 2003; De Lucia et al. 2006; Hopkins et al. 2010). In these models the formation of ETGs is directly linked to mergers events. The old stellar popula-

tions observed in almost all local ETGs suggest that most of the stellar mass formed a very long time ago and not during recent episodes of star formation (e.g. Thomas et al. 2005; Renzini 2006). This led to conclude that mergers that formed ETGs either occurred at very high redshift, $z > 4-5$, concurrently with or even triggering large episodes of star formation (e.g. Naab et al. 2007; Khochfar S. and Silk J. 2006a) or were "dry", that is the coalescence of pre-existing old stellar systems (e.g. De Lucia et al. 2006). In fact, the current and widely accepted view involves a combination of these two merger types acting at different time. Indeed, ETGs are thought to form at high redshifts as compact spheroids resulting from a main gas-rich merger event in which most of the stellar mass of the

* E-mail: paolo.saracco@brera.inaf.it

galaxy forms. They should then grow in size mostly by the addition a low stellar mass density envelope through subsequent dry minor mergers at later times (e.g. Hopkins et al. 2009; Naab et al. 2009; Bezanson et al. 2009). Naab et al. (2007) found that their simulated galaxies start forming stars at $z \approx 3 - 5$ concurrently with the intense phase of dissipative merging. In about 1.5 Gyr (at $z \sim 2.5$) almost 80 per cent of their final stellar mass is formed in the dissipative central starburst (see also Sommer-Larsen and Toft 2010) justifying the old stellar populations observed in local ETGs. Then, the resulting compact and massive spheroid grows in size through dry minor mergers whose main effect would be that of re-arranging stars mostly those far from the galaxy center, efficiently enlarging the size but keeping the inner parts and the total stellar mass of the galaxy nearly unchanged (e.g. Naab et al. 2009).

This scenario was triggered by the fact that the first observed high- z ETGs were characterized by an effective radius smaller than the mean radius of local counterparts with comparable mass, requiring a growth of their size across the time to match the size of the local ETGs. The above scenario, often called inside-out growth, qualitatively reproduces this possible size evolution of ETGs discussed and debated in many studies (Daddi et al. 2005; Trujillo et al. 2006; Longhetti et al. 2007; Trujillo et al. 2007; Cimatti et al. 2008; van der wel et al. 2008; van Dokkum et al. 2008; McGrath et al. 2008; Damjanov et al. 2009; Saracco et al. 2009; van der Wel et al. 2009; Trujillo et al. 2011; Damjanov et al. 2011; van de Sande et al. 2011). However, it requires a considerable fine tuning to reproduce both the local scaling relations and their scatter which is significantly smaller than the one produced by minor mergers (Nipoti et al. 2009; Nair et al. 2011). In addition to this argument, there are some observations that provide evidence that contradicts this stellar mass growth and the more general hierarchical scheme. Indeed, recent studies focused on brightest cluster galaxies at $1.2 < z < 1.5$ show that they were almost fully assembled by this time having already grown to more than 90 per cent of their final stellar mass at that redshift (Collins et al. 2009; Stott et al. 2010). In agreement with these results, studies on the evolution of the galaxy stellar mass function show that massive ETGs were already assembled at $z > 1$ and that they have not grown further at lower redshift (e.g. Pozzetti et al. 2010). These results suggest that merging has had little effect on the stellar mass growth of ETGs in the last 9 Gyr contrary to hierarchical models that predict a protracted mass build-up over Hubble time. Furthermore, in the last couple of years evidence of a large number of ETGs at $z \sim 1.5$ with sizes similar to those of local ones with comparable mass, here termed normal ETGs, has been accumulated showing that most of the high- z early-types were not more compact than local ones (Saracco et al. 2009; 2010; Mancini et al. 2010).

One of the differences between those works finding almost exclusively compact ETGs at high- z and those finding a majority of normal ETGs is the definition of early-type galaxy and, consequently, the selection criterion used to construct the samples of ETGs, a criterion that also determines the completeness of the samples, possible selection bias and the redshift range covered. The studies showing that the population of ETGs at high- z is composed of compact galaxies are based on samples of galaxies selected according to their colors and/or on samples of passive galaxies selected according to their low value of the specific star formation rate, a quantity derived from the best fits of their spectral energy distribution with stellar population synthesis models. These selection criteria allow the selectio of ETGs, according to the above definitions of ETG, even beyond $z \sim 2.5$ (e.g. Buitrago et al. 2008; Cameron et al. 2011; Cassata et al. 2011). The studies showing a

predominance of normal ETGs at high- z are based on morphologically selected samples and, for this reason, are usually limited to a slightly lower redshift ($z \sim 2$) than the former (e.g. Saracco et al. 2010; Mancini et al. 2010). We will discuss the implications that these different selection criteria of ETGs may have on the results in later sections of this paper.

Concurrently with the evidence of a large number of normal ETGs at $z \sim 1.5$, evidence of the presence of a large fraction of compact ETGs in the local Universe similar to the high- z ones has emerged (Valentinuzzi et al. 2010a; 2010b). In fact, the number density of compact ETGs morphologically selected at $z \sim 1.5$ is found to be consistent with the number density of ETGs selected in the same mass range in the local Universe (Saracco et al. 2010) showing that size evolution, if it exist, cannot affect the majority of the high- z ETGs, in agreement with what is found from other analysis (e.g. Newman et al. 2010; Stott et al. 2011). These recent results indirectly cast some doubt on the inside-out growth as a general mechanism of accretion of stellar mass and of growth in size. On the other hand, other studies focusing on the central and the effective stellar mass density of high- z ETGs have shown that the former is almost constant and similar to that observed in the local ETGs (e.g. Bezanson et al. 2009; van Dokkum et al. 2010; Tiret et al. 2011) providing one of the strongest arguments in favor of the hypothesized inside-out growth of ETGs throughout their life.

In this paper we focus on the central and the effective stellar mass density of ETGs and on their relations with other fundamental quantities. We use both a complete sample of ETGs at $0.9 < z_{spec} < 2$ and a local sample of ETGs selected according to the same criteria as used for the high- z sample in order to check for possible differences. The aim of this analysis is twofold. First, we want to asses whether the central and the effective stellar mass densities of ETGs are linked to the evolutionary path followed by ETGs and hence whether they can be used to probe their assembly history or whether they are independent on it. Secondly, we want to asses whether inside-out growth is a viable way to justify the properties observed in ETGs both at high- z and in the local universe examining both the evolution they underwent at $z < 1.5$ and the early phases they possibly experienced at $z > 2$. In Sec. 2 we describe the data. In Sec. 3 we define the central and the effective stellar mass densities probing the inside-out growth scenario at $z < 1.5$. In Sec. 4 we use the results obtained to constrain the general spheroids formation scheme at very early epochs. In Sec. 5 we define and study a scaling relation involving the central and the total stellar mass, scaling relation followed by ETGs independently of their redshift. Finally, in Sec. 6, we summarize the results and present our conclusions. Throughout this paper we use a standard cosmology with $H_0 = 70 \text{ Km s}^{-1} \text{ Mpc}^{-1}$, $\Omega_m = 0.3$ and $\Omega_\Lambda = 0.7$. All the magnitudes are in the Vega system, unless otherwise specified.

2 THE DATA SET

The sample of ETGs we used in our analysis is composed of 34 galaxies morphologically selected from the southern field of the Great Observatories Origins Deep Survey (GOODS-South; Giavalisco et al. 2004) described in Saracco et al. (2010). The sample was constructed by first selecting all galaxies brighter than $K \approx 20.2$ over the $\sim 143 \text{ arcmin}^2$ of the GOODS-South field and then by removing all the galaxies with measured spectroscopic redshift $z_{spec} < 0.9$ and those with irregular or disk-like morphology.

This first step of the morphological classification was undertaken through a visual inspection of the galaxies carried out independently by two of us on the ACS images in the F850LP band. Only galaxies for which the two independent visual classifications agree were removed. Then, on the basis of the best-fitting procedure to the observed profile described below, galaxies having a Sérsic index $n < 2$ or clear irregular residuals resulting from the fit were removed. Out of the 38 early-type galaxies thus selected 34 had measured spectroscopic redshift $0.9 < z_{\text{spec}} < 1.92$ leading to ~ 90 per cent spectroscopic completeness.

We note that at least eight galaxies of our sample show weak OII emission line (see Tab. 1). The lack of X-ray emission associated to these ETGs suggests that the emission is most probably associated with star formation rather than with AGN. Hence, these ETGs are not passive. Given the S/N (< 10) of the spectra at $\lambda_{\text{rest}} \approx 3500\text{\AA}-4000\text{\AA}$ and the continuum emission at these wavelengths, we estimate that only emission stronger than $\sim 10^{-18}$ erg $\text{cm}^{-2} \text{s}^{-1}$ could be detected. Thus, the star formation rate for these eight galaxies would be in the range 0.4-2 solar mass per year, according to their redshift, where we used the relation $\text{SFR}(M_{\odot} \text{ year}^{-1}) = (1.4 \pm 0.4) \times 10^{-41} \text{ L}[\text{OII}] (\text{erg s}^{-1})$ (Kennicutt 1998). It is worth noting that for masses of a few times $10^{10} M_{\odot}$ this would result in a specific star formation rate $-11 < \log(\text{SSFR}) < -10 \text{ yr}^{-1}$, higher than the SSFR often used to define passive galaxies (e.g. $\log(\text{SSFR}) \leq -11$ in Cassata et al. (2011)). We cannot exclude that the number of non-passive ETGs in our sample is higher than eight. Indeed, we note that the spectroscopic observations collected for these eight galaxies (di Serego Alighieri et al. 2005; Cimatti et al. 2008; van der Wel et al. 2005) are deeper than those of the other GOODS spectroscopic observations. Consequently, for many of them, in particular for those at $z > 1.4$, spectroscopic observations do not allow detection of OII emission lines fluxes as faint as a few 10^{-18} erg $\text{cm}^{-2} \text{s}^{-1}$, corresponding to $\text{SFR} \gg 1 M_{\odot} \text{ yr}^{-1}$ at that redshift. Hence, the presence of weak star formation would be hardly detectable. We note also that ETGs with colors bluer than those often used to select passive galaxies at $z > 1$ (e.g. $(R-K) > 5$, or $(I-H)_{AB} > 2.1$, Cameron et al. 2011) are present in our sample. All these ETGs, those non-passive and those bluer than the above color cuts, would not be included in a sample of ETGs selected according to their SSFR and/or to their colors. The resulting 34 ETGs of our sample are at redshift $0.9 < z_{\text{spec}} < 1.92$ and have stellar masses in the range $0.6 \times 10^{10} < M_{*} < 3 \times 10^{11} M_{\odot}$ as derived by fitting their spectral energy distribution (SED) sampled by 14 photometric points in the wavelength range 0.3-8.0 μm (Saracco et al. 2010).

3 THE CENTRAL AND EFFECTIVE STELLAR MASS DENSITIES OF ETGS

3.1 Surface brightness profile fitting

The effective radius R_e [kpc] (r_e [arcsec]) of our galaxies has been derived by fitting a Sérsic profile

$$I(R) = I_e \exp \left[-b_n \left[\left(\frac{R}{R_e} \right)^{1/n} - 1 \right] \right] \quad (1)$$

to the observed light profile in extremely deep (40-100 ks) HST ACS-F850LP images. The point spread function (PSF) to be convolved with the Sérsic profile has been constructed for each galaxy by averaging the profile of some unsaturated stars. The two-dimensional fitting has been performed using Galfit software (v. 2.0.3, Peng et al. 2002). The fitting to the galaxy profiles provided

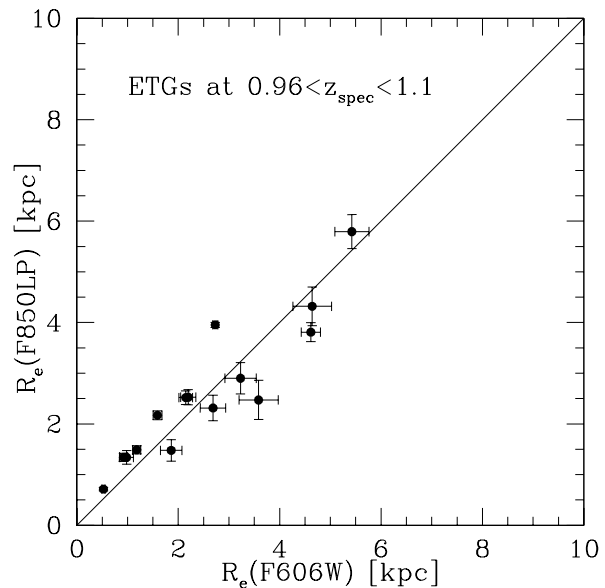


Figure 1. The effective radius of the 15 galaxies of our sample in the redshift range $0.96 < z < 1.1$, derived in the ACS-F850LP band ($\lambda_{\text{rest}} \sim 0.42 \mu\text{m}$) is compared to the effective radius derived in the ACS-F606W band ($\lambda_{\text{rest}} \sim 0.3 \mu\text{m}$).

us with the axial ratio b/a and the semi-major axis a_e of the projected elliptical isophote containing half of the total light which is related to the circularized (averaged) effective radius by the relation $r_e = a_e \sqrt{b/a}$. The effective radii R_e we obtained through the two-dimensional fitting procedure are in the range 0.4-9 kpc.

A concern over the effective radii thus derived could arise in relation to the different rest-frame wavelengths sampled by the F850LP filter given the wide redshift range of our sample. In particular, while at $z \sim 1$ the F850LP filter samples the rest-frame close to the B band ($\sim 0.42 \mu\text{m}$), at $z > 1.5$ this filter samples the rest-frame at $\sim 0.3 \mu\text{m}$, close to the U and NUV bands. However, the emission in the B and U bands of a galaxy is dominated by the light coming from the same young stellar component, in contrast to the emission at $\lambda_{\text{rest}} > 0.65-0.7 \mu\text{m}$ (R band) which is dominated by the old stellar component. Hence we do not expect a dependence of the size of our galaxies on the different rest-frame wavelength sampled, i.e. on the B-band or U-band according to the redshift of the galaxy. In order to exclude the presence of this dependence we selected the 15 galaxies of our sample in the redshift range $0.96 < z < 1.1$ and we compared their effective radius measured in the F850LP band, sampling $\lambda_{\text{rest}} \approx 0.42 \mu\text{m}$, with the effective radius measured in the F606W band, sampling $\lambda_{\text{rest}} \approx 0.3 \mu\text{m}$. The comparison is shown in Fig. 1. It can be seen that no dependence on wavelength is present as expected.

3.2 Stellar mass density estimates

In Fig. 2, the effective radius R_e of the 34 ETGs of our sample (filled symbols) is plotted as a function of their stellar mass M_{*} . The solid line is the local size-mass (SM) relation of Shen et al. (2003), while the dotted lines mark one sigma scatter. According to the definition already used in Saracco et al. (2010), cyan points represent the ETGs falling within one sigma from the local SM relation, here termed normal, while magenta points are compact ETGs, those falling at least 1 sigma below the relation. Crosses

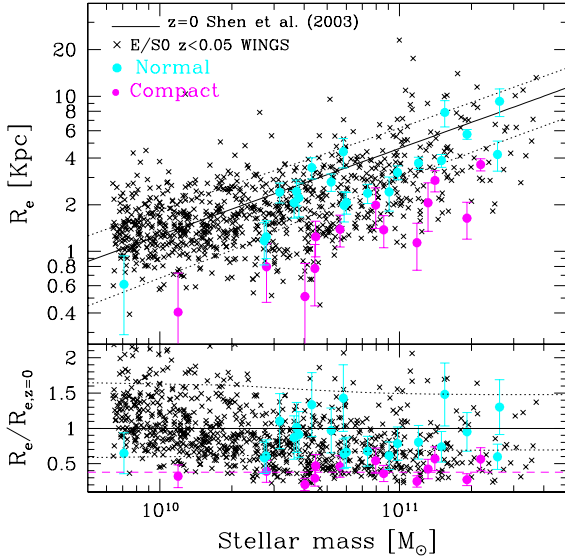


Figure 2. Upper panel: the effective radius R_e of the 34 ETGs at $0.9 < z_{\text{spec}} < 2$ (filled symbols) and of the ~ 900 ETGs selected from the WINGS survey (crosses) is plotted as a function of their stellar mass M_* . The solid line is the local size-mass (SM) relation by Shen et al. (2003) with its 1 sigma scatter (dotted lines). Cyan points are those high- z ETGs (normal) falling within one sigma from the local SM. Magenta points mark high- z ETGs more compact falling at least 1 sigma below the relation. Lower panel: the compactness, defined as the ratio between the effective radius R_e of the galaxy and the effective radius $R_{e,z=0}$ of an equal mass galaxy at $z=0$ as derived by the local SM relation, is plotted as a function of the stellar mass. Symbols are as in the upper panel.

represent ~ 900 ETGs we selected at $z < 0.05$ from the Wide-field Nearby Galaxy Cluster Survey (WINGS; Fasano et al. 2006; Valentinuzzi et al. 2010a). We point out that the local SM by Shen et al. is taken as reference to define normal and compact galaxies. It acts in the same way on any sample of ETGs considered. For instance, we used this relation to define compact ETGs both in our high- z sample and in the WINGS sample to compare in a consistent way their co-moving number density (Saracco et al. 2010). The local sample of ETGs has been selected from the WINGS sample in the same stellar mass range and on the basis of their morphology, as done for our high- z sample. In particular we selected ellipticals (E) and lenticulars (S0) according to the morphological classification of the WINGS survey (Fasano et al. 2012). It is worth noting that WINGS effective radii have been measured on the V-band images ($\lambda_{\text{rest}} \approx 0.5 \mu\text{m}$; Pignatelli et al. 2006), very close to our $\lambda_{\text{rest}} \sim 0.42 \mu\text{m}$). In the lower panel of Fig. 2, the compactness, defined as the ratio between the effective radius R_e of the galaxy and the effective radius $R_{e,z=0}$ of an equal mass galaxy at $z=0$ as derived by the local SM relation, is plotted as a function of the stellar mass for both the samples.

Integrating the best-fitting Sérsic profile of eq. (1) over a projected area $A = \pi R_1^2$ we derived for each galaxy the luminosity L_1 interior the radius $R_1 = 1$ kpc

$$L_1 = 2\pi I_e R_e^2 n \frac{e^{b_n}}{b_n^{2n}} \gamma(2n, x) \quad (2)$$

where n is the Sérsic's index, $x = b_n(R_1/R_e)^{1/n}$ and $\gamma(2n, x)$ is the incomplete gamma function. The choice of 1 kpc radius (2 kpc diameter aperture) within which to calculate the central stellar

mass density has been made in consideration of the resolution of the ACS-F850LP images characterized by a FWHM ≈ 0.15 arcsec corresponding to about 1.2 kpc at $z \sim 1$. However, it is important to note that the stellar mass densities are derived from the intrinsic galaxy profile, the Sérsic profile. Thus, PSF does not affect in any way the estimate of the stellar mass densities. PSF plays a role only in the 2-dimensional fitting to the observed profile as it is convolved with the Sérsic profile. By replacing in eq. (2) $\gamma(2n, x)$ with the complete gamma function $\Gamma(2n)$ we obtained the total luminosity L_{tot} (Ciotti 1991) and the fraction of luminosity interior to R_1 is then

$$\frac{L_1}{L_{\text{tot}}} = \frac{\gamma(2n, x)}{\Gamma(2n)}. \quad (3)$$

In our computation we assumed the analytic expression $b_n = 1.9992n - 0.3271$ (Capaccioli 1989) to approximate the value of b_n . Assuming that the light profile traces the stellar mass profile and that the mass-to-light ratio (M/L) is radially constant across the galaxy, the stellar mass M_1 interior to 1 kpc is given by $M_1 = L_1/L_{\text{tot}} \times M_*$, where M_* is the total stellar mass of the galaxy obtained from the SED fitting. Because the radius R_1 is fixed, the stellar mass density interior R_1 is $\rho_1 = cM_1$, where $c = (4/3\pi R_1^3)^{-1} = 0.239$ [kpc^{-3}]. Hence, ρ_1 and M_1 follows the same behavior of the other quantities. Under the same assumptions we also derived the effective stellar mass density $\rho_e = 0.5M_*/(4/3\pi R_e^3)$, that is the density interior the effective radius. The whole set of parameters used and derived in this work for the sample of 34 ETGs is summarized in Tab.1.

In fact, the mass-to-light ratio could not be radially constant for all the galaxies for the presence of color gradients in some high- z ETGs (e.g. Gargiulo et al. 2011, 2012; Guo et al. 2011). We investigated whether this can affect our estimate of stellar mass densities and our results. (U-R) $_{\text{rest}}$ color gradients in high- z ETGs, when present, are negative indicating a redder color toward the center of the galaxy. Gargiulo et al. (2012), using synthetic stellar population model fitting to different galaxy regions, find that the main driver of such color gradients is the age of the stellar populations, older toward the center than in the outskirts with a possibly higher metallicity. Older ages imply larger M/L values, higher metallicity lower M/L values. Thus the two parameters act in an opposite way regarding M/L canceling out each other, at least partially. Anyway, let us assume that only the age varies radially thus producing the maximum M/L radial variation. According to this, M/L should be larger toward the center with respect to the M/L we derived from the SED fitting averaged over the whole galaxy. Consequently, both the central stellar mass density and the effective mass density should be slightly higher. On the basis of the age gradients estimated by Gargiulo et al. (2012) we derived that the possible M/L variation is in the range 1-1.3. Thus, the central and the effective mass densities could be larger at most by this factor. In particular, for those galaxies whose effective radius is comparable to 1kpc (~ 12 galaxies in our sample) the effect will be exactly the same for both the stellar mass densities, central and effective. For the remaining galaxies whose effective radius $R_e \gg 1$ kpc the effect will be slightly larger for the central stellar mass density than for the effective density. Gargiulo et al. (2012) detect color gradients in 7 out of the 14 ETGs studied and find that color gradients are not related to the compactness of the galaxies. Thus, we expect that about 50 per cent of our sample show color gradients, independently of their compactness. It follows that, in the hypothesis of maximum M/L radial variation (i.e. of pure age variation) the distributions of the central and effective stellar mass densities could

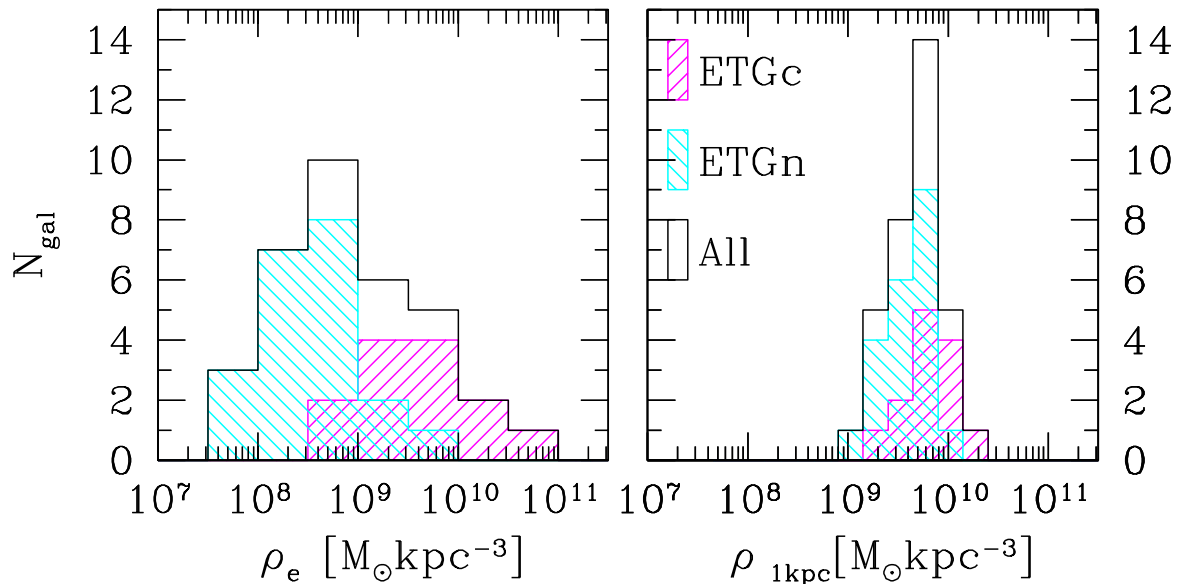


Figure 3. The distributions of the stellar mass density ρ_e within the effective radius (left panel) and of the central stellar mass density ρ_1 within 1 kpc radius (right panel) are shown for the whole sample of 34 ETGs at $0.9 < z < 2$ (solid histograms). The shaded histograms represent the distributions of normal ETGs falling within one sigma from the local size-mass (SM) relation (cyan) and of ETGs more compact falling at least 1 sigma below the relation (magenta).

be offset by a factor in the range 1-1.3. Thus, the assumption that M/L is radially constant for all the galaxies does not introduce any significant systematic in our analysis even in the case that it is not strictly true.

In Fig. 3 the distributions of the stellar mass density ρ_e within the effective radius (left panel) and of ρ_1 within 1kpc radius (right panel) are shown. The black solid-line histogram represents the distribution of the whole sample of 34 ETGs while the shaded histograms show the distribution of normal ETGs (cyan) and of compact ETGs (magenta). The distribution of the effective stellar mass density ρ_e of Fig. 3 (left panel) varies by about three orders of magnitude, from $\sim 10^8 M_\odot \text{ kpc}^{-3}$ to $\sim 10^{11} M_\odot \text{ kpc}^{-3}$ with a median value $\bar{\rho}_e = 7 \times 10^8 M_\odot \text{ kpc}^{-3}$, reflecting the large variation (a factor ~ 8) of R_e for ETGs of the same stellar mass visible in Fig. 2. In contrast, the distribution of the central mass density ρ_1 shown in the right panel of Fig. 3 spans just an order of magnitude centered at $\bar{\rho}_1 \simeq 5 \times 10^9 M_\odot \text{ kpc}^{-3}$. The values of ρ_1 are actually within a factor 2 from the median value as noted by other authors (e.g. Bezanson et al. 2009; Tiret et al. 2011). Analogously, while the median value ρ_e of normal ETGs ($3.5 \times 10^8 M_\odot \text{ kpc}^{-3}$) differs by a factor 10 from the median value ρ_e of compact ETGs ($3.9 \times 10^9 M_\odot \text{ kpc}^{-3}$) in the case of ρ_1 the median values differ by less than a factor 2 (4×10^9 vs $7 \times 10^9 M_\odot \text{ kpc}^{-3}$). This information is summarized in Fig. 4 where the central mass density ρ_1 of the 34 ETGs of our sample is plotted versus the effective mass density ρ_e (filled circles). Our data are best-fitted by the relation $\rho_1 \propto \rho_e^{0.1 \pm 0.1}$, in agreement with Tiret et al. (2011) (to an increase by two orders of magnitude of ρ_e corresponds an increase by a factor 1.5 of ρ_1) even if the correlation between the two quantities is not statistically significant being the probability of the Spearman rank test $P = 0.27$. The small variation of the central mass density of ETGs with respect to the large variation of the effective stellar mass density is often used to advocate the inside-out growth of stellar mass experienced

by ETGs through time (e. g. Bezanson et al. 2009; van Dokkum et al. 2010). In this scenario ETGs, after having assembled at high- z as compact/dense spheroids, gain a low stellar mass density envelope through subsequent dry minor mergers at later times growing efficiently in size and less in mass and reaching at $z = 0$ the typical size of local ETGs (e.g. Hopkins et al. 2009; Naab et al. 2009). In a plot like the one shown in Fig. 4, high- z ETGs would populate the right-hand side (high effective stellar mass densities) of the $[\rho_e, \rho_1]$ plane and should migrate towards lower effective stellar mass density, the left-hand side, at lower redshift keeping almost constant the central density ρ_1 . In fact, some works based on incomplete sample of high- z ETGs pre-selected on the basis of their red color show this kind of segregation (e.g. Bezanson et al. 2009). On the other hand, it has been shown that this selection criterion is strongly biased toward compact ETGs (see Fig. 2 in Saracco et al. 2010). To directly verify how color selection affects this plot, we selected the 10 reddest galaxies of our sample corresponding to a color $(F850LP-K)_{AB} > 2.4$. These galaxies are marked by a black filled square in Fig. 4. It is evident that they preferentially populate the right-hand side of the plot and thus that a color selection produce the segregation above. In contrast, it can be seen that the 34 ETGs morphologically selected at $z \sim 1.5$ of our sample are not segregated in the right-hand side of the plot but rather they span three order of magnitude in effective stellar mass density in spite of their high redshift. Furthermore, in Fig. 5 the effective radius, the stellar mass, the central and effective stellar mass density of the 34 galaxies of our sample are plotted as a function of their redshift. It can be seen that there are no significant correlation between these quantities and the redshift, as also confirmed by the Spearman rank test. Hence, our analysis and our conclusions cannot be affected by any possible dependence on redshift of these quantities. Actually, Fig. 5 suggests also that there is no significant evolution of R_e and ρ_e over the redshift range $0.9 < z < 2$. Thus, because at $z \sim 1.5$

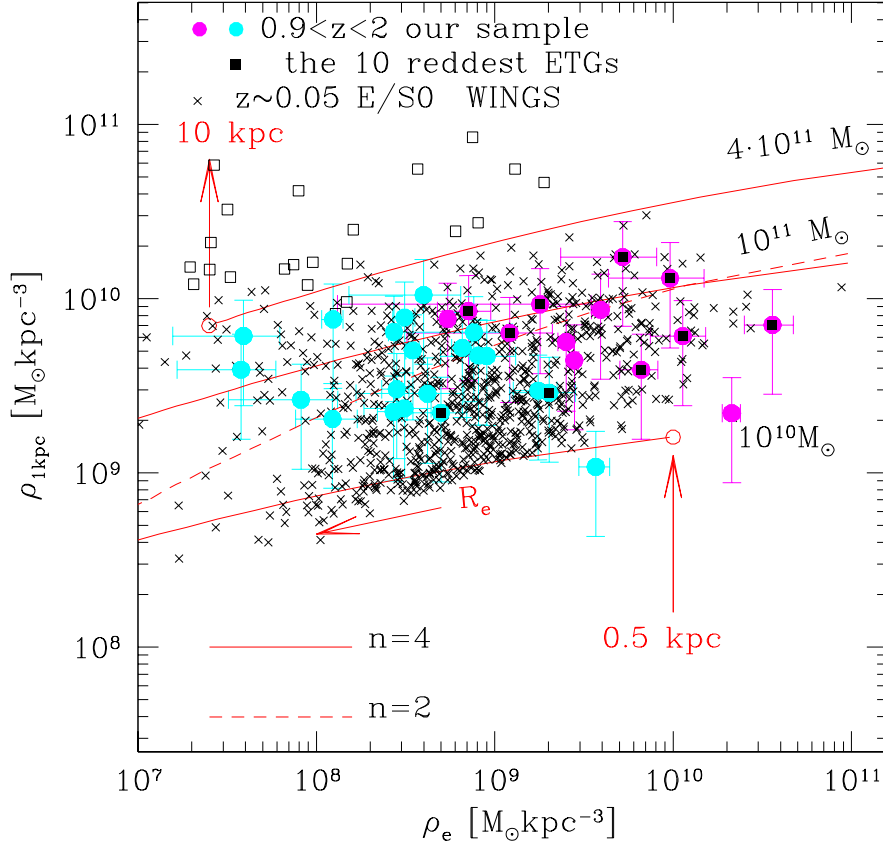


Figure 4. The stellar mass density within 1 kpc radius ρ_1 is plotted versus the effective stellar mass density ρ_e . Large filled dots represent the ETGs of our sample at $0.9 < z < 2$ (cyan normal ETGs, magenta compact ETGs). Black filled squares superimposed to filled dots mark the 10 reddest galaxies of our sample, i.e. galaxies with color $(F850LP-K)_{AB} > 2.4$. Black crosses represent the local ETGs selected from the WINGS sample. The open squares represent the 23 super-massive ($0.3 - 5 \times 10^{12} M_\odot$) ETGs selected by Bernardi et al. (2006; 2008) and studied by Tirit et al. (2011). The red lines represent the locus occupied on the $[\rho_e, \rho_1]$ plane by galaxies described by a Sersic profile with index $n = 4$, effective radii in the range $0.5 < R_e < 10$ kpc and stellar masses $10^{10} M_\odot$ (lower line), $10^{11} M_\odot$ (middle line) and $4 \times 10^{11} M_\odot$ (upper line) respectively. The dashed line is obtained for an index $n = 2$ and a mass $10^{11} M_\odot$.

co-exist compact ETGs and normal ETGs, if we accept the framework of the inside-out accretion of stellar mass we must conclude that the latter must have increased their radius at earlier epochs, at $z > 2$, while the former will increase their size later, at lower redshift. In the next section we compare this observational evidence with the inside-out growth accretion proposed to assemble ETGs.

4 PROBING THE INSIDE-OUT GROWTH OF ETGS

4.1 Are the central and the effective stellar mass densities related to the assembly history of ETGs ?

Whether or not a fraction of the local ETGs have undergone a similar mass accretion in the last 9-10 Gyr ($z < 1.5-2$), to properly consider the observed variations of the central and the effective stellar mass densities of ETGs, one must take into account the following property: if the light profile of a galaxy and hence its stellar mass profile is represented by a Sersic profile (eq. 1) with index $n > 2$ then the mass density within a fixed radius (e.g. 1 kpc) and the effective stellar mass density are related exactly as shown by the data in Fig. 4, independently of redshift and of mass accretion experienced. This is shown in Fig. 4 by the red solid lines. The lower solid

line represents the locus occupied on the $[\rho_e, \rho_1]$ plane by galaxies described by a Sersic profile with index $n = 4$, having stellar mass $10^{10} M_\odot$ and effective radii in the range $0.5 < R_e < 10$ kpc. The middle and the upper solid lines represent galaxies with the same parameters but having a stellar mass $10^{11} M_\odot$ and $4 \times 10^{11} M_\odot$ respectively. We see also that the lower the Sersic index the stronger the correlation between ρ_1 and ρ_e as shown by the steeper dashed line obtained for an index $n = 2$ (normalized to $10^{11} M_\odot$). Both the stellar mass range and the effective radius range considered to compute the curves are those covered by our data. We see that the effective stellar mass density of these simulated galaxies spans about three orders of magnitude while the central mass density ρ_1 is constrained within an order of magnitude. Thus, any galaxy described by a set of parameters $[n, M_*, R_e]$ within the above intervals ($n > 2$, $M_* = 0.1 - 4 \times 10^{11} M_\odot$, $R_e = 0.5 - 10$ kpc) will lie between the upper and the lower lines independently of redshift and of accretion history. In fact, our high- z ETGs fall between the two lines and spans the range bound by the two curves. In order to verify the independence of redshift of this evidence we used the ~ 900 early-type galaxies at $z < 0.05$ selected from WINGS survey. We computed the central mass density ρ_1 and the effective mass density ρ_e of these ETGs using the same procedure described above and used for our high- z sample. The ~ 900 local ETGs are shown

in Fig. 4 as crosses. As expected, they fall in the region bounded by the two red lines covering the same distribution as the high- z sample. Fig. 4 also shows the 22 super-massive ($0.3 - 5 \times 10^{12} M_{\odot}$) ellipticals selected by Bernardi et al. (2006; 2008) on the basis of their high velocity dispersion ($\sigma_v > 330$ km/s) and studied by Tirit et al. (2011) (open squares). It can be seen that these ETGs follow the same behavior shown by the other data: a central stellar mass density almost constant (but centered at a higher value according to the higher stellar mass range) and a large variation of ρ_e . Finally, it is also important to note from Fig. 4 that the effective stellar mass density, the quantity which is expected to change dramatically (as the cube of the variation of R_e) in the inside-out scenario from high- z to low- z , is not different in the two samples considered, in agreement with what is shown by our high- z sample in the lower panel of Fig. 5. This is more clearly shown in Fig. 6 where the distribution of the effective stellar mass density of our sample at $0.9 < z < 2$ is compared to the distribution of ρ_e of the WINGS ETGs. The two distributions are equal as confirmed by the Kolmogorov-Smirnov test which provides a probability $P=0.85$. Thus, these results show two main facts. The first one is that, all the ETGs independently of redshift and of their accretion history have the mass density interior to a fixed radius within a narrow range of values if compared to the stellar mass density within the effective radius. This fact reflects a peculiar feature of the true intrinsic profile shape that they follow which is very well reproduced by a Sersic profile (see also Graham and Driver 2005). Since this behavior depends on the intrinsic profile shape of ETGs, it follows that also non-parametric estimators, e.g. Petrosian radius, would return qualitatively the same results. Thus, whether or not an ETG formed as a compact spheroid its central stellar mass density will fall within a narrow range of values depending only on its total stellar mass. It does not depend on any past assembly history and has no connection with the possible inside-out growth. The other important evidence is that the effective stellar mass density of early type galaxies, the quantity expected to decrease dramatically in the inside-out growth scenario as the effective radius increases, has not changed in the last 9-10 Gyr. This implies that the large spread of ρ_e and of R_e observed both in the local universe and up to $z \sim 1.5 - 2$, as shown in figures 2, 3 and 4, must originate earlier, at $z > 2$.

4.2 Stellar mass densities and the evolution of ETGs at $z > 2$: toward the early-phases of their assembly

Figures 4 and 6 clearly show that the properties of the local ETGs in terms of stellar mass and stellar mass densities were already in place at $z \sim 1.5 - 2$. For this reason such properties must necessarily be the product of the evolutionary path followed by ETGs at $z > 2$, in the previous 2.5-3 Gyr i.e. during the assembly of most of their mass. Before making any hypothesis, let's see whether the general scheme of compact spheroids formation and evolution described above can justify the spread of the effective stellar mass density observed at $z \sim 1.5 - 2$. From figures 2 and 4 we see that, at a given mass, there are galaxies with effective radii (effective stellar mass densities) differing even by a factor 5-6 (more than hundred) even if all of them have nearly the same central mass density. Thus, in the hypothesis that ETGs formed first as compact spheroids, those galaxies that at $1 < z < 2$ have large radii (5-6 times larger) with respect to others with equal mass, had to increase their size at an earlier epoch, at $z > 2$. Hence, the inside-out accretion should have been extremely efficient at $z > 2$, in the first 2-3 Gyr of the universe to produce so many large galaxies in so short time. Some authors have already discussed this point in different contexts (e.g. Nipoti

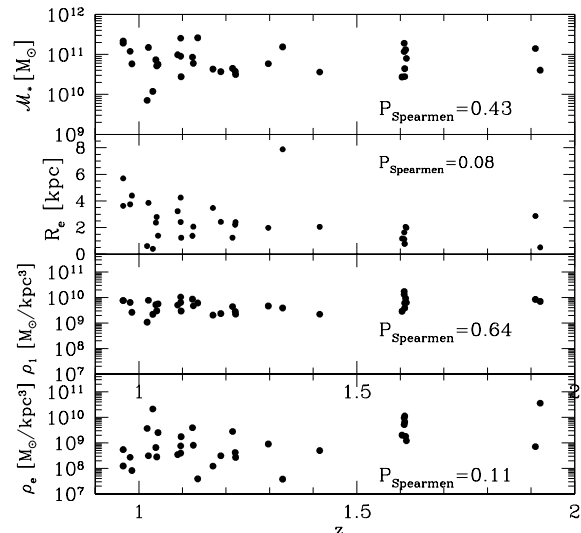


Figure 5. From top: the stellar mass M_* , the effective radius R_e , the central stellar mass density ρ_1 and the effective stellar mass density ρ_e of the 34 ETGs of our sample at $0.9 < z_{spec} < 2$ are plotted as a function of their redshift. No significant correlation is present. $P_{Spearman}$ is the probability that the two quantities are not correlated as resulting from the Spearman rank test.

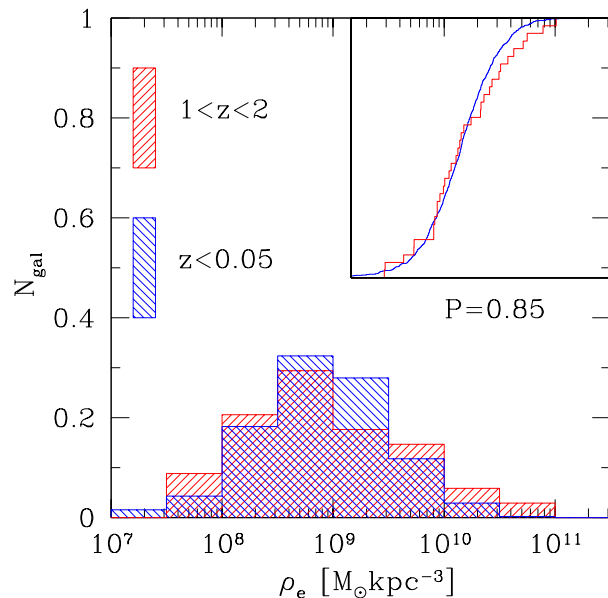


Figure 6. The distribution of the effective stellar mass density of ETGs at $0.9 < z < 2$ (red histogram) is compared to the distribution of the effective stellar mass density of the local ETGs selected from the WINGS survey (blue histogram). The effective stellar mass density is the quantity expected to dramatically change in the inside-out growth scenario of ETGs. The two distributions are equal as confirmed by the Kolmogorov-Smirnov test.

et al. 2009; Newman et al. 2011; Saracco et al. 2011) concluding that the required dry merging does not seem to be consistent with model predictions. Here, we can directly give an estimate of the merger rate needed on the basis of the observed data. Let us consider a galaxy of our sample having effective radius (effective stellar mass density) 4 (~ 60) times larger than another galaxy of equal mass at the same redshift. Let us assume that dry minor merger is very efficient in increasing the size of galaxies, as efficient as proposed by Naab et al. (2009) where the effective radius grows by the square of the change in mass instead of linearly. The larger galaxy has already increased its radius by a factor 4 during its life at $z > 2$. To increase the radius by a factor 4 the larger galaxy had to double at least its mass at $z > 2$. In the case of mergers involving galaxies with masses, e.g., $M : m \leq 1 : 5$ (1:10), the galaxy had to undergo five (ten) mergers in the previous ~ 2.5 Gyr (between $2 < z < 6$) to double its mass. Thus, the resulting merger rate per galaxy would be about 2 (4) mergers per Gyr. If the final stellar mass at $z \sim 1.5-2$ of the larger galaxy was $10^{11} M_{\odot}$ the progenitor should have a mass $M \sim 5 \times 10^{10} M_{\odot}$ at $z > 2$. Using the merger rate calculator by Hopkins et al. (2010) we estimated at $z = 2.5$ a merger rate per galaxy of about $6 \times 10^{-3} \text{ Gyr}^{-1}$ for masses in the range $5 \times 10^{10} - 10^{11} M_{\odot}$. We considered dry merging, i.e. mergers involving gas fractions up to 10% of the total mass (gas+stars). The predicted merger rate would be even lower for lower masses ($6 \times 10^{-4} \text{ Gyr}^{-1}$ for masses $< 5 \times 10^{10} M_{\odot}$), for higher redshift ($3 \times 10^{-3} \text{ Gyr}^{-1}$ at $z = 3$) and for lower mass ratios ($4 \times 10^{-3} \text{ Gyr}^{-1}$ for $M : m \leq 1 : 10$). Thus, the required merger rate at $z > 2$ as directly derived from the observed data to justify the data themselves in the hypothesis of accretion through minor mergers, is three orders of magnitude higher than the one predicted by models. Moreover, such high merger rates are excluded also from the merger rate derived from the observations of galaxy pairs at high- z . For instance, López-Sanjuan et al. (2011) estimate a minor merger rate $R_{\text{mm}} \sim 0.04 \text{ Gyr}^{-1}$ at $z \sim 0.8$ and they find that it should decrease with increasing redshift. Thus, at $z \sim 1.5$ we should expect a minor merger rate $R_{\text{mm}} < 0.04 \text{ Gyr}^{-1}$, more than two orders of magnitude lower than the one required above.

Some recent studies which find almost exclusively compact ETGs at high- z contrary to our observational evidence, consider the possibility that this difference is due to the higher redshift range covered by their samples. For instance, Cassata et al. (2010) and Szomoru et al. (2011) estimate the size of ETGs at $1.5 < z < 2.5$ using WFC3 data (0.13 arcsec/pix vs FWHM ~ 0.15 arcsec) finding almost all compact ETGs. They select (and define) ETGs according to their colors and/or specific star formation rate. A possible suggested explanation for the higher fraction of normal ETGs observed at lower redshift ($z \sim 1 - 1.5$) is that some of the compact ETGs at high- z increase their size between $z \sim 2.5$ and $z \sim 1.5$, i.e. in about 1.5 Gyr. However, if this was the case, following the same reasoning as above, a galaxy should have experienced from five to ten mergers in about 1.5 Gyr, requiring a merger rate of 3-7 Gyr^{-1} at $1.5 < z < 2.5$, even higher than the one excluded before. It seems then that the different fraction of compact galaxies they found with respect to our sample cannot be accounted for by this hypothesis but rather it should be attributed to other factors. For these works, particular attention should be paid to the different criteria used to define and hence to select early-type galaxies. In this regards, it is worthwhile to mention the work by van der Wel et al. (2011). They investigated the stellar structure of massive, quiescent galaxies in the redshift range $1.5 < z < 2.5$ using HST-WFC3 images. They found that their effective radii were actually smaller than ETGs in the present-day universe with equal stellar mass. However, they estimate that 65 \pm 15 per cent of the population of massive quiescent

galaxies at $z \sim 2$ are disk dominated. Thus, the hypothesis of an inside-out growth driven by dry merging does not seem a viable mechanism to justify the large spread of the effective radius and of the stellar mass densities characterizing the population of ETGs at $1 < z < 2$. To reinforce this conclusion it is also the detection of color gradients high- z ETGs (Gargiulo et al. 2011; Guo et al. 2011) In particular, Gargiulo et al. (2012) detect color gradients in some but not all the ETGs of the sample at $1 < z < 2$. Most importantly, they find that the presence or the absence of color gradients is not related to the compactness of the galaxy: color gradients are presents both in compact and in normal ETGs as well as some of the ETGs, both compact and normal, do not show color gradients. Necessarily, inside-out growth driven by dry merging cannot be assumed as a general scheme of accretion but a different scenario must be hypothesized. We further analyzed the properties of high- z ETGs in order to gain new insights and constraints on the possible mechanism(s) able to produce the observed properties.

5 CENTRAL STELLAR MASS DENSITY AND SCALING RELATIONS

In the left panel of Fig. 7 the central stellar mass density ρ_1 is plotted versus the stellar mass M_* of the galaxies. It is evident the tight correlation between the two quantities. The correlation is well reproduced by the relation

$$\rho_1 = 2.35(\pm 0.3) \times 10^3 M_*^{0.58 \pm 0.16}. \quad (4)$$

for our high- z ETGs (filled circles). We note that the local sample of ETGs (crosses) follow the same correlation with a best-fitting relation possibly slightly steeper ($\rho_1 \propto M_*^{0.73}$). It is worth noting that Tirit et al. (2011) found an opposite correlation using their data set ($\rho_1 \propto M_*^{0.25}$), in contrast with our result and also with what the data of the other authors they used show (see their Fig. 6). There are two main differences between their work and the others which could justify this discrepancy. The first one is that they consider the sample of super-massive ellipticals ($0.3 - 5 \times 10^{12} M_{\odot}$) with velocity dispersion larger than 330 km s^{-1} (Bernardi et al. 2006), while the other samples (as well as our own) include galaxies less massive with no cuts in velocity dispersion. The other difference is the stellar mass estimator used to derive the density within 1 kpc. Indeed, while we and the other authors have used the light profile to derive the fraction of stellar mass within a fixed radius, they use a dynamical mass computed by solving the Jeans equation. To directly verify whether the different stellar mass range characterizing their sample can justify the different result, we derived the central stellar mass density of their ETGs according to our method (using eq. 2) using the stellar mass they obtain from stellar population model (column 6 in their Tab. 2). Their sample is represented in figures 7 by open squares. It is evident in this case the agreement of their data with the others data in all the cases, showing that the different mass range and the selection in velocity dispersion are not the reasons of their opposite correlation. We believe that the use of the dynamical mass they define is the reason of the different result. Actually, their Fig. 4 shows the large scatter which exists between the dynamical mass and the stellar mass they derived and a relation between them slightly steeper than 1:1 which could be the reasons of the different behavior they find. The result obtained from this comparison shows that the correlation between the central stellar mass density and the stellar mass discussed above and the resulting considerations are valid for the population of ETGs independently of redshift, of mass and of velocity dispersion ranges considered.

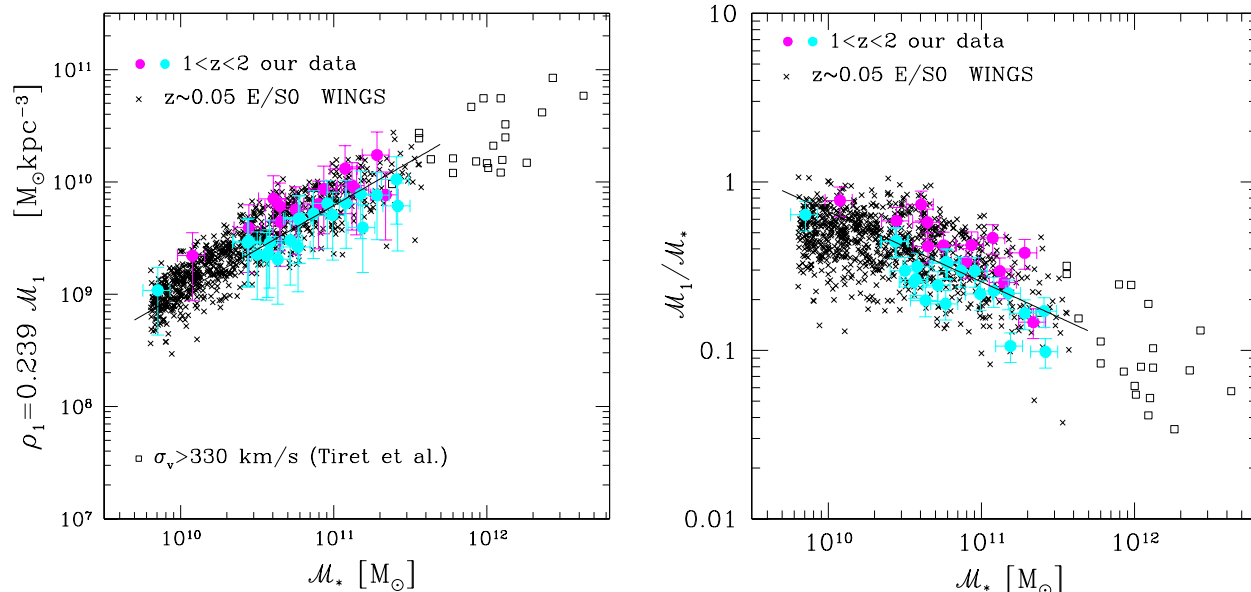


Figure 7. Left - The central stellar mass density ρ_1 is plotted versus the total stellar mass M_* for our sample of high- z ETGs (large filled magenta and cyan circles) and for the WINGS sample of local ETGs (black crosses). These two quantities are tightly correlated independently of the redshift and the compactness of the galaxies. The correlation is well represented by eq. (4). Right - The fraction of the stellar mass within 1 kpc radius is plotted versus the total stellar mass of the galaxy. Symbols are the same as in the left panel. The existence of the correlation shown in the left panel and of the form of eq. (4) implies the correlation shown in this plot: the fraction of stellar mass contained within 1 kpc radius decreases with increasing total stellar mass of the system (eq. (5)).

Because $\rho_1 = 0.239M_1$, it follows that also the central stellar mass increases with the total stellar mass of the galaxy according to the same scaling relation, $M_1 \propto M_*^{0.58}$. Furthermore, from the above relation it follows that the fraction of the central stellar mass decreases with mass as

$$M_1/M_* = 9.85M_*^{-0.42} \quad (5)$$

Hence, if the stellar mass of the galaxy increases by a factor two then the stellar mass and the density within 1 kpc increase more slowly, by a factor 1.5. Consequently, the fraction of stellar mass contained within 1 kpc, M_1/M_* , decreases by a factor 1.3 when the total mass double as shown in the right panel of Fig. 7. Finally, it is interesting to note that since the effective radius of ETGs increases with mass as $R_e \propto M_*^{0.56}$ (e.g. Shen et al. 2003) and $\rho_1 \propto M_*^{-0.6}$ (eq. 4) it follows that ρ_1 is nearly independent of R_e , as it is. This is another and independent way to show that ρ_1 and ρ_e are nearly uncorrelated, independent of redshift and of assembly history since the relations used to derive this correlation are valid both for high- z ETGs and for local ETGs independently of their compactness. Moreover, this indirectly shows that the small variation of the central stellar mass density of ETGs with respect to the effective mass density is an intrinsic characteristic of the Sersic's profile and has no regards with the inside-out growth.

In all the cases considered above there are no differences between the high- z sample and the local sample in spite of the extra 9 Gyrs for local ETGs compared with high- z ETGs. All the ETGs follow the tight correlations shown above independently of their compactness and of their redshift. Hence, whatever evolution experienced by ETGs during the last 9-10 Gyr of their life, must be able to leave their properties unchanged. Such properties, already in place at $z \sim 1.5 - 2$, must necessarily originate at earlier epoch, during the first 3 Gyr. The large spread of the effective stellar mass density equally observed in the ETGs at $z \sim 1.5$ and in the local ETGs representing our large variation of R_e at fixed stellar

mass, must originate in the early-phases of their formation. And the mechanism(s) responsible for mass growth of ETGs must proceed according to the above scaling relations.

6 SUMMARY AND CONCLUSIONS

We studied the relations between the stellar mass density within the effective radius ρ_e and the stellar mass density within a fixed radius of 1 kpc ρ_1 for a complete sample of 34 ETGs at $0.9 < z_{spec} < 2$ with stellar masses in the range $0.6 \times 10^{10} - 3 \times 10^{11} M_\odot$. As previously found by other authors (e.g. Tiret et al. 2011; Bezanson et al. 2009) we find that the central stellar mass density ρ_1 of ETGs varies just by a factor of two and it is similar to the one of local ETGs. This property of the high- z ETGs was supposed to be the sign of the spheroid formation scenario in which ETGs assemble at high- z as compact/dense spheroids and then add a low stellar mass density envelope growing efficiently in size and less in mass. The central stellar mass density and the stellar mass of the galaxy would remain nearly constant while the effective stellar mass density would strongly decrease across the time as the effective radius increases. However, we find that the effective stellar mass density ρ_e of high- z ETGs varies by almost 3 orders of magnitude exactly as the local ETGs. We find indeed that high- z and low- z ETGs selected in the same stellar mass range populate the same locus in the $[\rho_e, \rho_1]$ plane and that the distribution of the effective stellar mass density did not change since $z \sim 1.5$, i.e. in the last 9-10 Gyr. This implies that the large spread of ρ_e observed both in the local universe and up to $z \sim 1.5-2$ must originate earlier, at $z > 2$. Moreover, we show that the small variation of the central stellar mass density with respect to the large variation of the effective density does not depend on redshift and/or on the past assembly history. On the contrary, this feature is characteristic of the Sersic profile. Thus, the relation between the stellar mass densities of ETGs is not represen-

Table 1. For each galaxy of the sample we report the spectroscopic redshift, the total apparent magnitude F850LP_{fit} resulting from the best fitting profile on the HST-ACS images, the effective radius R_e , the Sérsic index n , the effective stellar mass density ρ_e measured within the effective radius, the central stellar mass density ρ_1 measured within 1 kpc radius, the total stellar mass M_* and the stellar mass M_1 within 1 kpc, the mean age of the stellar population. We remind that $\rho_1 = 0.239M_1$. The last column (OII)_{em} reports those galaxies showing OII emission.

ID	z_{spec}	F850LP _{fit} [mag]	R_e [kpc]	n	$\log\rho_e$ [$M_\odot \text{ kpc}^{-3}$]	$\log\rho_1$ [$M_\odot \text{ kpc}^{-3}$]	$\log M_*$ [M_\odot]	$\log M_1$ [M_\odot]	Age Gyr	(OII) _{em}
472	1.921	23.84	0.51±0.03	2.4	10.51	9.80	10.56	10.42	1.02	–
2361	1.609	23.31	1.14±0.10	4.0	9.90	10.03	10.99	10.66	3.25	(1)
2148	1.609	22.75	1.64±0.15	4.8	9.61	10.13	11.17	10.75	3.50	–
2111	1.610	23.33	0.78±0.04	3.5	9.97	9.71	10.57	10.33	1.02	–
12	1.123	21.08	1.38±0.03	4.9	9.47	9.81	10.81	10.43	2.40	–
11322	1.032	22.08	0.41±0.01	3.0	10.25	9.27	10.00	9.89	1.02	–
2543	1.612	23.91	2.06±0.32	3.2	9.13	9.84	11.00	10.47	3.00	(1)
2355	1.610	23.67	0.80±0.03	2.1	9.78	9.55	10.40	10.17	0.90	–
3	1.044	20.98	1.39±0.02	4.9	9.26	9.62	10.62	10.24	2.00	–
12294	1.215	21.55	1.24±0.01	1.8	9.40	9.60	10.60	10.22	1.02	(2)
2196	1.614	22.92	1.99±0.24	4.8	8.93	9.65	10.75	10.27	1.68	–
4	0.964	19.98	3.63±0.03	2.4	8.71	9.86	11.31	10.48	3.00	–
11804	1.910	22.97	2.87±0.16	4.5	8.71	9.78	11.00	10.41	0.90	–
11539	1.096	20.20	4.25±0.44	4.0	8.55	9.97	11.36	10.60	2.75	–
11	1.096	21.46	2.42±0.25	5.0	8.88	9.81	10.96	10.43	3.25	(3)
2286	1.604	23.72	1.17±0.08	2.2	9.25	9.40	10.38	10.02	1.14	(1)
9369	1.297	22.27	1.98±0.15	4.7	8.92	9.64	10.74	10.26	2.30	–
12327	1.097	22.15	1.24±0.06	4.8	9.13	9.36	10.33	9.98	1.90	–
8	1.125	21.48	2.07±0.04	5.0	8.79	9.55	10.66	10.18	2.10	–
11888	1.039	20.97	2.37±0.05	4.8	8.69	9.59	10.74	10.21	2.50	–
20	1.022	20.41	3.85±0.09	5.4	8.32	9.72	11.00	10.34	2.75	–
12965	1.019	22.72	0.61±0.02	3.8	9.49	8.95	9.77	9.58	1.14	–
1	1.089	20.34	3.23±0.05	3.9	8.41	9.57	10.86	10.19	0.81	(3)
13	0.980	19.83	3.75±0.04	5.5	8.30	9.67	10.94	10.29	1.61	–
2	0.964	19.69	5.69±0.13	5.7	7.92	9.71	11.11	10.33	2.60	–
2239	1.415	23.26	2.06±0.14	2.0	8.62	9.27	10.48	9.89	1.14	(1)
12789	1.221	22.55	2.21±0.22	5.0	8.47	9.31	10.43	9.93	2.40	–
23	1.041	21.19	2.80±0.08	3.9	8.29	9.32	10.56	9.94	1.90	–
9066	1.188	22.45	2.43±0.16	3.5	8.36	9.24	10.44	9.86	2.50	–
12000	1.222	22.06	2.41±0.08	5.0	8.35	9.27	10.42	9.89	1.14	(2)
7	1.135	20.28	9.29±0.93	5.0	7.49	9.69	11.32	10.31	2.60	–
10414	1.170	21.87	3.47±0.22	3.7	7.91	9.13	10.46	9.75	2.40	–
12434	1.330	21.31	7.88±0.74	4.6	7.32	9.34	10.93	9.96	1.80	–
14	0.984	20.73	4.40±0.44	5.0	7.69	9.20	10.54	9.82	1.70	–

(1) Cimatti et al. (2008); (2) di Serego Alighieri et al. (2005); (3) van der Wel et al. (2005)

tative and cannot be used to probe their past assembly history. It has no connection with the inside-out growth. We investigated whether the spread of the effective radius and of the effective stellar mass density observed in ETGs up to ~ 1.5 can be the sign of the inside-out growth taken place at higher redshift ($z > 2$). We find that the number of mergers needed to justify at $z \sim 1.5$ a spread of a factor 4 in R_e or about 60 in ρ_e is from five to ten in the redshift range $2 < z < 6$, corresponding to a merger rate of about 2-4 Gyr⁻¹. This merger rate is three orders of magnitude higher than the one predicted by models and than the one derived from the observations of high- z galaxy pairs.

As also discussed in Saracco et al. (2011), a scenario where the main starburst triggered by the dissipative gas-rich merging is the main driver of the stellar mass growth, could qualitatively account for the observations when supposing that gas cooling can modulate the star formation. Indeed, assuming that dissipative gas-rich merger at high- z ($z > 4 - 5$) is the main mechanism of spheroids formation, compact ETGs would be a natural consequence of this mechanism when most of the gas at disposal is burned in the central starburst, that is when the gas is sufficiently cold to collapse

toward the center and to ignite the main starburst. On the contrary, when the gas of the progenitors is not sufficiently cold and homogeneous the resulting starburst would not be short, central and intense but longer and possibly composed of many episodes. The cooling time of the gas clouds and their orbital parameters could modulate the rate at which the starburst(s) are ignited, stoked and distributed across the galaxy.

We find and define a tight correlation between the central stellar mass density of ETGs and the total stellar mass in the sense that the central stellar mass density increases with mass as $M_*^{-0.6}$. We find that this correlation is general and it is valid for the whole population of ETGs, independently of redshift, mass and/or of velocity dispersion ranges considered. Given this correlation it follows also that the fraction of the central stellar mass of ETGs decreases with mass.

The large spread of the effective stellar mass density equally observed in the ETGs at $z \sim 1.5$ and in the local ETGs representing the large variation of R_e at fixed stellar mass, must obviously originates at $z > 2$. The fact that this property apparently did not change in the subsequent 9-10 Gyr as it is equally observed in the local

ETGs, suggest that it must have originated during the early phases of their formation. Moreover, whatever the evolution ETGs underwent during the last 9-10 Gyr of their life, such evolution must be able to leave unchanged their properties and the correlation found.

ACKNOWLEDGMENTS

This work is based on observations made with the ESO telescopes at the Paranal Observatory and with the NASA/ESA Hubble Space Telescope, obtained from the data archive at the Space Telescope Science Institute which is operated by the Association of Universities for Research in Astronomy. We thank B. Poggianti, A. Moretti, T. Valentini and the WINGS team for having provided us with their data. We would like to thank the referee, John Stott, for useful and constructive comments which improved the quality of the paper. This work has received financial support from ASI-INAF (contract I/009/010/0).

7 REFERENCES

- Bernardi, M., et al. 2006, *AJ*, 131, 2018
 Bernardi, M., Hyde, J. B., Fritz, A., Sheth, R. K., Gebhardt, K., Nichol, R. C. A., 2008, *MNRAS*, 391, 1191
 Bezanson R., van Dokkum P. G., Tal T., Marchesini D., Kriek M., Buitrago F., Trujillo I., Conselice C. J., Bouwens R. J., Dickinson M., Yan H. 2008, *ApJ*, 687, L61
 Cameron E., Carollo C. M., Oesch P. A., Bouwens R. J., Illingworth G. D., Trenti M., Labbé I., Magee D., 2011, *ApJ*, 743, 146
 Capaccioli, M. 1989, in *World of Galaxies (Le Monde des Galaxies)*, 208
 Cassata P., et al. 2010, *ApJ*, 714, L79
 Cassata P., et al. 2011, *ApJ*, 743, 96
 Cimatti A., et al. 2008, *A&A*, 482, 21
 Ciotti L., 1991, *A&A*, 249, 99
 Collins C. A., et al. 2009, *Nature* 458, 603
 Daddi E., Renzini A., Pirzkal N., et al. 2005, *ApJ*, 626, 680
 Damjanov I., McCarthy P. J., Abraham R. G., et al. 2009, *ApJ*, 695, 101
 Damjanov I., et al. 2011, *ApJ*, 739, L44
 De Lucia G., Springel V., White S. D. M., Croton D., Kauffmann G. 2006, *MNRAS*, 366, 499
 di Serego Alighieri S., et al. 2005, *A&A*, 442, 125
 Fasano G., et al. 2006, *A&A*, 445, 805
 Fasano G., et al. 2012, *MNRAS* 420, 926
 Gargiulo A., Saracco P., Longhetti M. 2011, *MNRAS*, 412, 1804
 Gargiulo A., Saracco P., Longhetti M. La Barbera F. 2012, *MNRAS*, submitted
 Giavalisco M., et al. 2004, *ApJ* 600, L103
 Graham A. W., Driver S. P., 2005, *PASA*, 22, 118
 Guo Y., et al. 2011, *ApJ*, 735, 18
 Hopkins, P., Bundy, K., Murray N., Quataert E., Lauer T. R., Ma C.-P. 2009, *MNRAS*, 398, 898
 Hopkins, P., et al. 2010, *ApJ*, 715, 202
 Kennicutt R. C. Jr., 1998, *ARA&A* 36, 189
 Khochfar S., Burkert A., 2003, *ApJ*, 597, L11
 Khochfar S., Silk J. 2006a, *ApJ*, 648, L21
 Longhetti M., Saracco P., Severgnini P., et al., 2007, *MNRAS*, 374, 614
 López-Sanjuan C., et al. 2011, *A&A*, 530, 20
 Mancini, C., Daddi E., Renzini A., et al. 2010, *MNRAS*, 401, 933
 McGrath E., Stockton A., Canalizo G., Iye M., Maihara T. 2008, *ApJ*, 682, 303
 Naab T., Johansson P. H., Ostriker J. P., Efstathiou G. 2007, *ApJ*, 658, 710
 Naab T., Johansson P. H., Ostriker J. P. 2009, *ApJ*, 699, L178
 Newman A. B., Ellis R. S., Treu T., Bundy K. 2010, *ApJ*, 717, L103
 Nair P., van den Bergh S., Abraham R., 2011, *ApJ*, 734, L31
 Nipoti C., Treu T., Auger M. W., Bolton A. S. 2009, *ApJ*, 706, L86
 Peng C. Y., Ho L. C., Impey C. D., Rix H.-W., 2002, *AJ* 124, 266
 Pignatelli E., Fasano G., Cassata P., 2006, *A&A*, 446, 373
 Pozzetti L., et al. 2010, *A&A* 523, 13
 Renzini A., 2006, *ARA&A*, 44, 141
 Saracco P., Longhetti M., Andreon S., 2009, *MNRAS*, 392, 718
 Saracco P., Longhetti M., Gargiulo A. 2010, *MNRAS*, 408, L21
 Saracco P., Longhetti M., Gargiulo A. 2011, *MNRAS*, 412, 2707
 Shen S., et al., 2003, *MNRAS*, 343, 978
 Sommer-Larsen J., Toft S., 2010, *ApJ*, 721, 1755
 Stott J. P., et al. 2010, *ApJ* 718, 23
 Stott J. P., Collins C. A., Burke C., Hamilton-Morris V., Smith G. P., 2011, *MNRAS*, 414, 445
 Szomoru D., Franx, M., van Dokkum P. G., 2011, *ApJ* 735, L22
 Thomas D., Maraston C., Bender R., Mendes de Oliveira C. 2005, *ApJ*, 621, 673
 Tirit O., Salucci P., Bernardi M., Maraston C., Pforr J. 2011, *MNRAS*, 411, 1435
 Trujillo I., Feulner G., Goranova Y., et al. 2006, *MNRAS*, 373, L36
 Trujillo I., Conselice C. J., Bundy K., Cooper M. C., Eisenhardt P., Ellis R. S., 2007, *MNRAS*, 382, 109
 Trujillo I., Ferreras I., de La Rosa I. G. 2011, *MNRAS*, 415, 3903
 Valentini P., et al. 2010a, *ApJ*, 712, 226
 Valentini P., et al. 2010b, *ApJ*, 721, L19
 van der Wel A., M. Franx, P. G. van Dokkum, H.-W. Rix, G. D. Illingworth, P. Rosati, 2005, *ApJ*, 631, 145
 van der Wel A., Holden B. P., Zirm A. W., Franx, M., Rettura, A., Illingworth G. D., Ford H. C., 2008, *ApJ*, 688, 48
 van der Wel A., Bell E. F., van den Bosch F. C., Gallazzi A., Rix H. 2009, *ApJ*, 698, 1232
 van der Wel A., et al. 2011, *ApJ* 730, 38
 van de Sande J., et al. 2011, *ApJ* 736, L9
 van Dokkum P. G., et al. 2008, *ApJ*, 677, L5
 van Dokkum P. G., et al. 2010, *ApJ*, 709, 1018
 Wuyts S., et al. 2010, *ApJ* 722, 1666